Observations of preferential summer melt of Arctic sea-ice ridge keels from repeated multibeam sonar surveys

Evgenii Salganik[1,2], Benjamin A. Lange[1,3], Christian Katlein[4], Ilkka Matero[4,5], Philipp Anhaus[4], Morven Muilwijk[1], Knut V. Høyland[2], Mats A. Granskog[1]

[1]Norwegian Polar Institute, Tromsø, 9296, Norway
[2]Norwegian University of Science and Technology, Trondheim, 7491, Norway
[3]Norwegian Geotechnical Institute, Oslo, 0484, Norway
[4]Alfred-Wegener-Institut Helmholtz-Zentrum für Polar- und Meeresforschung, Bremerhaven, 27570, Germany
[5]Svalbard Integrated Arctic Earth Observing System Knowledge Centre, Longyearbyen, 9171, Svalbard

Correspondence to: Evgenii Salganik (evgenii.salganik@proton.me)

Abstract. Sea-ice ridges constitute a large fraction of the total Arctic sea-ice area (up to 40–50 %); nevertheless, they are the least studied part of the Arctic ice pack. Here we investigate sea-ice melt rates using rare repeated underwater multibeam sonar surveys that cover a period of one month during the advanced stage of sea-ice melt. We show that the degree of bottom melt increases with ice draft for first-year and second-year level ice, and a first-year ice ridge, with an average of 0.45 m, 0.55 m, and 0.95 m of total snow and ice melt in the observation period, respectively. We investigated Arctic first-year ice ridge with 4.6 m average keel draft, 42 m width and 4 % macroporosity. While bottom melt rates of ridge keel were 4 times higher than first-year level ice, surface melt rates were almost identical and responsible for 40 % of ridge draft decrease. We show high spatial variability of ridge keel cross-sectional melt ranging from 0.2 m to 2.6 m with the maximum point ice loss of 6 m. We attribute 57 % of the ridge total melt variability to keel draft (36 %), slope (32 %), and width (27 %), with higher melt for ridges with larger draft, steeper slope and smaller width. The melt rate of ridge keel flanks was proportional to the draft, while there was increased keel melt within 10 m of its bottom corners, and the melt rates of the keel bottom were comparable to level ice melt.

1 Introduction

According to the definition by the World Meteorological Organization, an ice ridge is a line or wall of broken ice that is forced up by pressure (WMO, 2014). Ridges consist of a sail above and a keel below the water level. The keel initially consists of rubble, randomly packed ice blocks separated by water-filled voids, described by the ridge macroporosity (fraction of water-filled voids in the rubble). The initial macroporosity of first-year ice ridges is in the range of 20 % to 45 % (Bowen and Topham, 1996), with an average porosity of 30 % (Timco and Burden, 1997). Some ridges become fully consolidated (with near-zero macroporosity) during the melt season (Marchenko, 2022). Ice ridges are key features in climate studies since they constitute around 30 % of the total Arctic sea-ice volume (Rothrock, 2005). While Mårtensson et

al. (2012) used a multicategory sea ice model to estimate the Arctic sea-ice ridge volume of 45–60% and ridge area of 25–45 %.

Melling & Riedel (1996) observed an increase in ridge areal fraction from 15 % in autumn to 40–50 % in spring based on subsea sonar ice draft measurements in the Beaufort Sea in 1991–1992. However, the proportion of ridges varies depending on the region and how they are defined. Fram Strait serves as the main outlet of the Arctic sea ice export (Krumpen et al., 2016), and for that region Hansen et al. (2014) estimated the fraction of deformed ice of 37±8 %, using an evolving threshold relative to the modal thickness using draft measurements from moored upward-looking sonars during 1990–2011. In those observations, the ridge fraction increased in 1990–2008 and decreased thereafter, which was confirmed by Sumata et al. (2023) using extended data from the same upward-looking sonars in Fram Strait for 1990 to 2020. Sea-ice ridges can be formed from new, young, first-year, second-year, or multiyear level ice or from a combination of ice types. Typically, ridges are made from relatively thin ice (Tucker et al., 1984), which breaks as the weakest points during deformation events. Ridges themselves can also be first-year, second-year, or multiyear, depending on how many seasons they have survived. The maximum keel draft is limited by the ice strength and is correlated with adjacent level ice draft (Amundrud et al., 2004). Once the keel has reached its maximum possible draft, it thereafter only grows in width (Hopkins, 1998).

Previous research has suggested that ridges impact the melt rates of the ice. For instance, Rigby and Hanson (1976) showed enhanced bottom melt of a ridge keel in comparison to thinner ice, although mechanical erosion could not be ruled out for this rather deep ridge (order of 10–12 m). During the SHEBA expedition in the Beaufort and Chukchi Seas, Perovich et al. (2003) used data from single-point measurements from ablation stakes, and measured 60 % higher bottom melt for second-year and multiyear ice ridges (42 stakes) than for multiyear level ice (89 stakes) during the entire melt season from early June to early October 1998. Similarly, Skyllingstad et al. (2003) measured enhanced vertical mixing and a five-fold increase in ocean heat flux (OHF) for 10-m-deep ridge during winter season at SHEBA expedition, however, this does not take into account the shallow meltwater stratification that develops in summer and affects ice melt rates. Amundrud et al. (2006) estimated that ridge keels melt 4–5 times faster than level ice based on the observations from ice-profiling sonars mounted on subsea moorings in the Beaufort Sea (however, their data does not repeatedly measure the same ice). Furthermore, Shestov et al. (2018) observed ridge melt in summer during the N-ICE2015 expedition (Granskog et al., 2018) in the pack ice north of Svalbard using a single-point measurements from a temperature buoy. Here, the average OHF under level ice was 63 W m^{-2} (Peterson et al., 2017), while the ridge keel melted by 1.5 m over two weeks, which translates into an equivalent OHF of 300 W m^{-2}, 4.8 times higher than for level ice (Shestov et al., 2018). Based on the thermodynamic model developed by Amundrud et al. (2006), several parameters, such as keel width and shape, may impact keel melt, with ridge macroporosity and block thickness being key factors. Thus, the observed ratio of ridge and level ice accumulated melt in previous studies ranged from 60 % to 400 % even for similar geographical locations, suggesting the need of a more detailed investigations of spatial and temporal variability of melting of different ice types.

The first direct measurements of under-ice topography were linear profiles from narrow-beam upward-looking sonar (Lyon, 1961). Wadhams et al. (2006) and Wadhams & Doble (2008) were the first to use an autonomous underwater vehicle

65 instrumented with a multibeam sonar to study the three-dimensional bottom topography of Artic sea ice. Using multibeam mapping by a submarine, Wadhams & Toberg (2012) found a mean slope of first-year and multi-year ridge keels of 28° and 25°, respectively, assuming a triangular shape. Ekeberg et al. (2015) analysed the shape of ridge keels using data from upward-looking sonar in Fram Strait and suggested that ridge keels typically have a trapezoidal shape with the keel bottom width accounting for an average of 17 % of the keel total width.

70 Although ridges play an important role in the evolution of the Arctic ice pack, ridges are understudied compared to the level ice that is usually sampled. Aforementioned studies are also typically limited to a one-time snapshot and few point measurements. Furthermore, ridges have also been identified as potential biological hotspots (Gradinger et al., 2010; Fernández-Méndez et al., 2018) and influencing the light conditions beneath the ice (Katlein et al., 2021). The measurements collected in the Artic Ocean during the Multidisciplinary drifting Observatory for the Study of the Arctic Climate (MOSAiC)

75 expedition (Nicolaus et al., 2022) showed that complete consolidation of ridges may occur during spring season before the melt onset through the transfer of snow into ridge keels via open leads (Salganik et al., 2023a) or ice deformation, which was supported by 6 %–11 % estimates of snow mass fraction within several ridges (Lange et al., 2023). In this study we use novel repeated multibeam ice draft measurements that follow the temporal and spatial evolution of a first-year sea-ice ridge and adjacent level ice during summer melt collected in the Arctic Ocean during the MOSAiC expedition in 2020. Over a

80 period of a month, we observed ice draft changes and melt rates for first- and second-year level ice and a first-year ice ridge. Additionally, we identified key characteristics of ice bottom topography that affected the melt rates. The use of underwater multibeam sonar allows to collect over 10^5 measurements of sea ice draft with over 10^4 ridge draft measurements every week. In comparison to point measurements from temperature buoys (Shestov et al., 2018), ice coring and ablation stakes (Perovich et al., 2003), ROV sonar measurements increase the amount of draft data points by three orders of magnitude,

85 revealing small-scale spatial variability of sea ice melt at unprecedented detail. In comparison to moored subsea sonar ice draft measurements (Amundrud et al., 2006), Repeated ROV surveys allowed us to study the same sea ice repetitively for a longer period with high spatial resolution and with reduced uncertainty in measured melt rates.

2 Materials and Methods

2.1 Expedition

90 The MOSAiC expedition took place in 2019–2020 to better understand the coupled Arctic ice, ocean, and atmosphere system and the sea-ice mass and energy budget over a full season and included a range of snow and sea ice measurements (Nicolaus et al., 2022). The MOSAiC Central Observatory, approximately 3 km by 4 km large ice floe, drifted for 10 months across the central Arctic starting from 4 October 2019, following the Transpolar Drift, until it reached the ice edge in Fram Strait and broke apart on 31 July 2020 (Fig. 1c). The OHF estimate from ice mass balance buoys (IMBs) increased from

95 11 W m^{-2} to 40 W m^{-2} during July 2020 (Salganik et al., 2023b), with an average value of 24 W m^{-2}, comparable to the summer OHF estimates of 20–30 W m^{-2} for Beaufort Gyre and Transpolar Drift in 1979–2002 (Krishfield, 2005). The OHF

increase took place in mid-July, coinciding with a reduction in sea ice concentration from 100% to 85% within a 3 km radius of the Central Observatory (Krumpen et al., 2021). This decrease in sea ice led to a higher solar heat input and hence warming of the mixed layer (Fig. 1b). Despite the floe also drifting further south into Fram Strait and getting closer to
100 shallower and warmer Atlantic Water at the same time, the mixed layer and upper ocean conditions still retained their Arctic characteristics. This is evident through the observation of remarkably low heat fluxes over the halocline (-0.01 ± 0.3 W m^{-2}) and thermocline ($+2.1\pm1.2$ W m^{-2}) in Fram Strait (Schulz et al., in prep.).

Due to logistical reasons, the ridge investigations during MOSAiC were performed at several sites. During January–July 2020, Alli's Ridge was studied using ice coring and IMBs, while in June–July 2020 Jaridge was studied using IMBs,
105 underwater sonar surveys and ice coring. The measurements of Alli's Ridge draft included only 4 ice coring sites visited before and during melt season (Salganik et al., 2023a) and will be used only as a reference for Jaridge investigations.
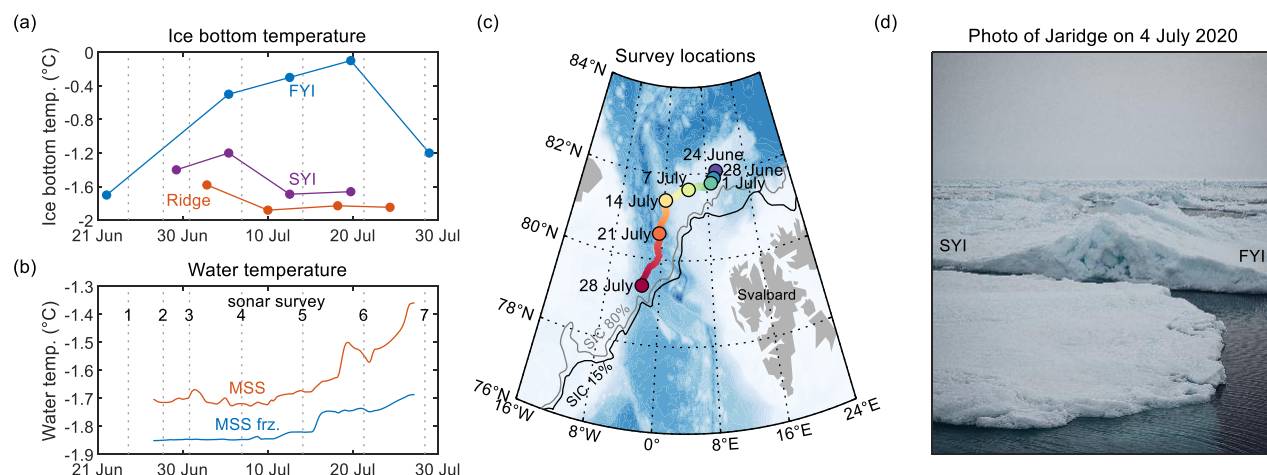
Figure 1: (a) Ice bottom temperature for first-year ice (FYI), second-year ice (SYI) and ridge from coring; (b) water temperature and water freezing temperature from microstructure profiles (MSS) at 5-m depth; (c) overview map of the study area with drift of
110 the MOSAiC ice floe for ROV multibeam sonar observations from 24 June to 28 July 2020; (d) surface photography with the investigated ice ridge internal sail structure on 4 July 2020. Displayed ice edges in (c) were derived from AMSR-2 sea-ice concentration (SIC) product for thresholds of 15 % and 80 % on 28 July 2020 (Spreen et al., 2008).

2.1 Ridge drilling

In this study, we focus primarily on the evolution of a ridge called 'Jaridge'. Jaridge was formed between 4–12 February
115 2020 based on the visual inspection of sea-ice surface elevation models from an airborne laser scanner (Jutila et al., 2022). The ice blocks forming the ridge were 0.2–0.4 m thick (Fig. 1d), the average sail height was 0.5 m, and the average draft was 3.8 m. It was formed between level first-year ice and level second-year ice. We investigated ridge morphology using a 2-inch diameter ice auger (Kovacs Enterprise, USA). Ice drilling was organized along seven drilling transects perpendicular to the ridge crest orientation (Fig. 2a). Each transect contained 3–7 drilling locations with measurements of ice draft, freeboard,
120 depth of ridge voids, and snow thickness at a horizontal spacing of 2.5 or 5 m (Fig. 2b). The ridge was measured seven times (25 June to 29 July) during the summer melt season when located over the Yermak Plateau and Fram Strait (79.4–82.1° N,

2.8° W–10.2° E, Fig. 1b). Jaridge covered 12 % of the area of sonar surveys which included four classified ice types (Fig. 2c). Another shallower ridge, 'Porridge' was also located within the survey area but only mapped with the multibeam sonar. The area at the top right quarter of sonar surveys was heavily covered with false bottoms during 7–29 July (Salganik et al.,

125 2023b) and was therefore excluded from our analysis. Temperature, salinity, and isotope compositions from Jaridge coring are presented in Lange et al. (2023).
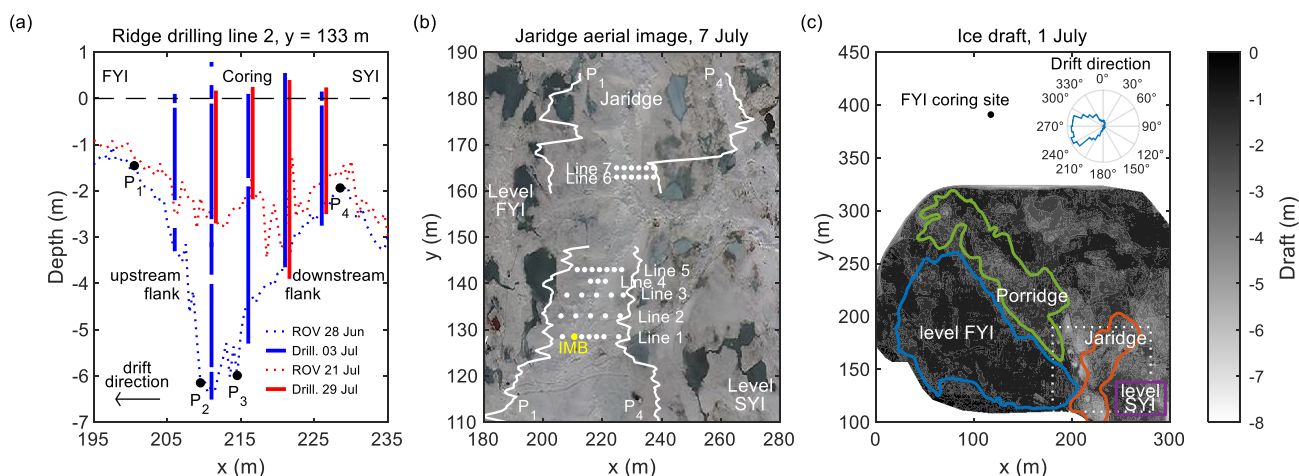
Figure 2: (a) Cross-section of ice draft in late June and late July 2020 along drilling line 2; (b) locations of ridge drillings, ice mass balance buoy (IMB) and keel width boundaries of Jaridge on an aerial image from 7 July; (c) ice bottom topography on 1 July
130 **2020, measured by remotely operated vehicle (ROV) multibeam sonar, showing location of first-year ice (FYI), second-year ice (SYI), Jaridge and Porridge and location of (b) inside white dotted-line box. The polar histogram in (c) shows frequency of ice drift direction in relation to the displayed ice floe orientation, with prevailing drift in western direction.**

To study the temporal evolution of the ridge interfaces, we used temperature measurements from IMB 2020M26 (Bruncin d.o.o.). The IMB consisted of a 5-m-long chain with a sensor spacing of 2 cm and provides temperature readings every 6

135 hours with an accuracy of 0.1°C. The IMB was installed on 26 June 2020, at the ridge drilling Line 1 (Fig. 2b). At deployment, the consolidated layer thickness was 1.9 m, keel depth was 4.0 m, and snow depth was 0.6 m. To study the evolution of level ice draft, thickness, and interface evolution, we also used data from the first-year ice (FYI) coring site located 70 m away from the ridge surveys (Fig. 2c), further detailed in Salganik et al. (2023b). These observations include a combination of IMB temperature measurements and sea-ice coring conducted on a weekly basis, with measurements of FYI

140 temperature, salinity, and density, as well as snow and ice thickness and draft from 20–30 sea-ice cores per week.

2.2 Underwater multibeam sonar

We use measurements from a multibeam sonar (DT101, Imagenex, Canada) mounted on a remotely operated vehicle (ROV, M500, Ocean Modules, Sweden, after Katlein et al. (2017)) to measure ice draft in an area of approximately 350 m by 200 m, with 0.05 m draft accuracy and horizontal resolution of 0.5 m. Seven surveys at a depth of 20 m were performed

145 during the melt season (24 June to 28 July), close to the floe edge of the Central Observatory of MOSAiC (Nicolaus et al.,

2022), covering an area with undeformed ice and several ice ridges including the Jaridge (Fig. 1c). In our analysis we mostly use the first six sonar surveys, as ice deformations decreased co-location accuracy of sea ice ridges for the last survey.

2.3 Ridge morphology analysis

To quantify how ridge characteristics affect the melt rates, we divided our ridge draft multibeam observations into 131
150 individual cross-sections which were nearly parallel to the direction of ice drift during June–July. The distance between neighbouring cross-sections was 0.5 m. We determined the following characteristics for each cross-section: keel bottom width, draft, slope, and distance from the keel front. To quantify these parameters with a single value, we simplified each cross-section to a trapezoidal shape following Ekeberg et al. (2015). Four points of these trapezoids (P_1–P_4, Fig. 2a) coincide with the largest transition of the smoothed inclination of ridge cross-sections, separating each cross-section into upstream
155 flank, keel bottom, and downstream flank (locations of P_1 and P_4 are shown in Fig. 2b). The upstream flank was facing the ice drift direction, while the downstream flank was on the leeside of the prevailing ocean current relative to the ice (Fig. 2c). The keel bottom width is equal to the horizontal projection of the keel bottom (P_2–P_3), while the keel draft equals to the average draft of the keel bottom. The keel slope is defined as the angle between the upstream flank and the waterline. A tangent line, "touching" the position of all P_2 points of cross-sections (upstream bottom corners), is the keel front (Fig. 4c).
160 The distance from P_2 of each cross-section to the keel front was identified as one of the factors for studying ridge melt rates.

3 Results and discussion

3.1 Level ice melt

In this study, we focus on the observed difference in sea-ice draft between the sonar surveys from 24 June to 21 July due to large spatial variability in melt rates. During this period, an area of undeformed FYI (Fig. 2c) with an initial draft of
165 1.4±0.2 m experienced a 0.42±0.26 m decrease in draft, while an area of undeformed SYI with an initial draft of 2.6±0.7 m decreased by 0.50±0.31 m (20 % more than FYI). A shallow ridge ('Porridge') with an initial draft of 2.3±0.8 m (similar to SYI) experienced a 0.54±0.61 m decrease in draft. FYI draft decrease had a positive correlation with its initial draft, with a regression slope of 0.47. Such relationship may be related to the strong vertical stratification of the ocean mixed layer observed in July (Fer et al., 2022). Skyllingstad et al. (2003) suggested that fresh water insulate sea ice if turbulent mixing is
170 weak, while thicker ice and ridges are efficient at forcing turbulence in the fresh layer. This agrees with our measurements of FYI, SYI and ridge bottom temperatures (Fig. 1a), where thinner ice was stronger affected by meltwater for a longer time, which led to a lower OHF.

3.2 Ridge morphology and keel melt

Repeated ridge drilling showed that Jaridge keel melt was very variable (Fig. A1). The average melt along ridge drilling
175 lines 1–5 (Fig. 2b) was 1.7 m, while ridge flanks melted up to 4.5 m. For the ROV sonar surveys, the average draft change of

the ridge area was 0.9±1.0 m with an average initial draft of 3.9±1.1 m (Fig. A2). The maximum ridge draft decreased from 8.2 m to 7.0 m, while the largest observed ridge draft reduction of 6.1 m. The average keel slope was 14–15° for both flanks, half of that reported by Wadhams & Toberg (2012), possibly because of the larger 5 m minimum ridge draft threshold used in their study. The average fraction of keel bottom width (P_2–P_3, Fig. 2a) to keel width (P_1–P_4) was 38 %, twice as large as

180   the 17 % estimated by Ekeberg et al. (2015), possibly related to the larger keel bottom draft (7.2 m in comparison to our 5.3 m). Co-location of ridge draft measurements from drilling and from sonar showed a good agreement of the two draft measurement techniques (R^2 = 0.8, Fig. A1). According to the individual observations of ice draft evolution from sonar, the melt of ridge flanks stronger (1.7 times larger regression slope) depended on ice draft in comparison to the keel bottom (Fig. 2b). The average melt at the same depth was higher for flanks than for keel bottom. For example, for an ice draft larger than

185   4 m, the average draft change for upstream flank, keel bottom, and downstream flank was 1.3 m, 1.0 m, and 1.4 m, respectively. Fig. 2b can be used to predict the ridge melt relative to level ice melt depending only on ridge draft and fraction of keel bottom width. On average, ridge flanks and keel bottom were melting 1.7 and 2.0 times faster than FYI at the coring site. Higher average melt rate for keel bottom was related to higher average initial draft for keel bottom (4.4 m) than for flanks (3.1 m).
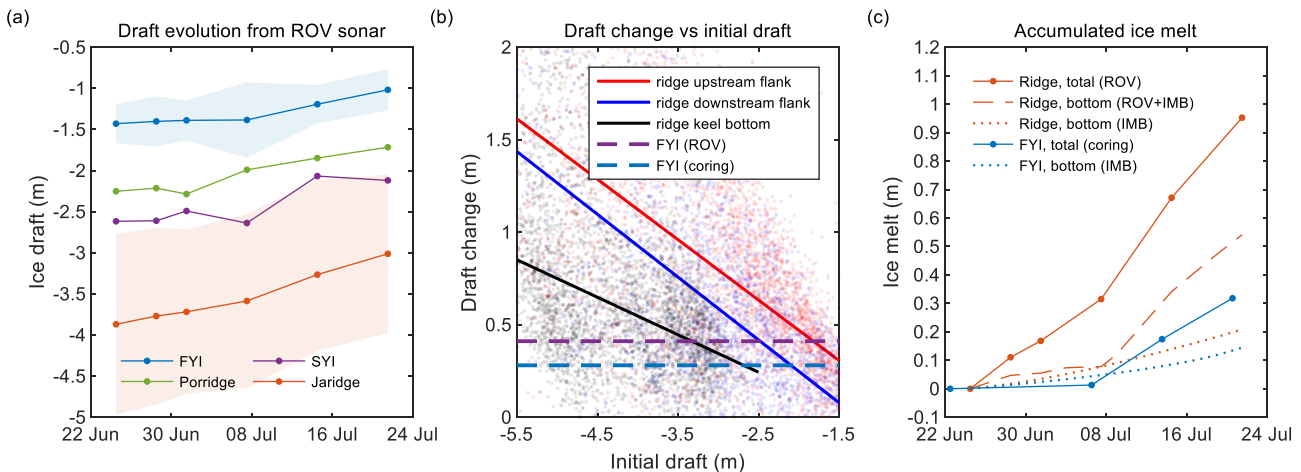
Figure 3: (a) Evolution of the average sea-ice draft measured by a ROV multibeam sonar for first-year ice (FYI), second-year ice (SYI), Porridge and Jaridge during June–July 2020; **(b)** draft change for single-point sonar measurements of ridge upstream and downstream flanks and keel bottom, corresponding linear regression with solid lines, and average draft change for FYI coring site; **(c)** accumulated ice melt for ridge and FYI estimated from ROV multibeam sonar, ice mass balance buoy (IMB) and ice coring measurements. Shaded areas in (a) represent standard deviations of draft measurements.

3.3 Ridge cross-sectional melt

Based on the results of multiple linear regression analysis, keel draft, slope, bottom width and distance to the keel front (Fig. 4c) are responsible for 57 % (coefficient of determination R^2) of ridge melt variability with 37 % positive correlation with keel draft, 32 % positive correlation with keel slope, 27 % negative correlation with keel bottom width, and 11 % negative

200   correlation with distance from the keel front. The roughness of the ridge keel, characterized by its draft standard deviation,

did not have a significant effect on the ridge melt. The large correlation of ridge melt with its draft may be explained by a combination of both higher ice melt and lower keel width for larger drafts. Based on ridge drilling observations from this study and from another examined ridge during MOSAiC (Salganik et al., 2023a), the flanks of ridge keels are usually less consolidated, which may be coupled with higher ocean turbulence at the ridge flanks in comparison to the keel bottom.

205 The keel bottom width ranged from 1 m to 35 m with an average of 13±9 m, and the highest melt was observed around ridge left and right bottom corners (P_2 and P_3) within diameter of 10 m (Fig. 4a). For wide profiles, it was possible to distinguish keel melt around two bottom corners and in the keel bottom between them. While areas within 10 m around upstream bottom corner (P_2) melted on average by 1.2 m, keel bottom without 10 m surroundings around both corners (P_2 and P_3) melted by 0.5 m (similar to level ice melt rates despite a much larger ice draft). We also found that all ridge cross-sections that had both

210 narrow keel bottom width and low keel melt were located within two areas (Fig. 4c) and were characterized by large distance from the keel front. Exclusion of profiles from these two areas would increase correlation (R^2) between keel melt and keel bottom width from 27 % to 57 % alone (Fig. 4b). We suggest that these areas were protected by the keel front from the turbulent fluxes, which appear to occur in the vicinity of ridge bottom corners (P_2 and P_3 in Fig. 2a). The ridge at y = 148–160 m was not trapezoidal and consisted of separate blocks with patchy draft evolution. This area with mechanical erosion

215 was not included into the correlation analysis but was included into the further comparison of level ice and ridge melt. The mean draft decrease for this area was 1.0±2.1 m, 10 % higher than for the rest of the ridge. The draft decrease of other ridge parts was gradual, suggesting little mechanical erosion. The strong negative correlation between keel melt and keel bottom width may be explained by the stronger ridge consolidation at its interior parts (Salganik et al., 2023a; Shestov et al., 2018), as well as by the smaller fraction of the keel affected by the enhanced turbulence around the keel bottom corners P_2 and P_3.
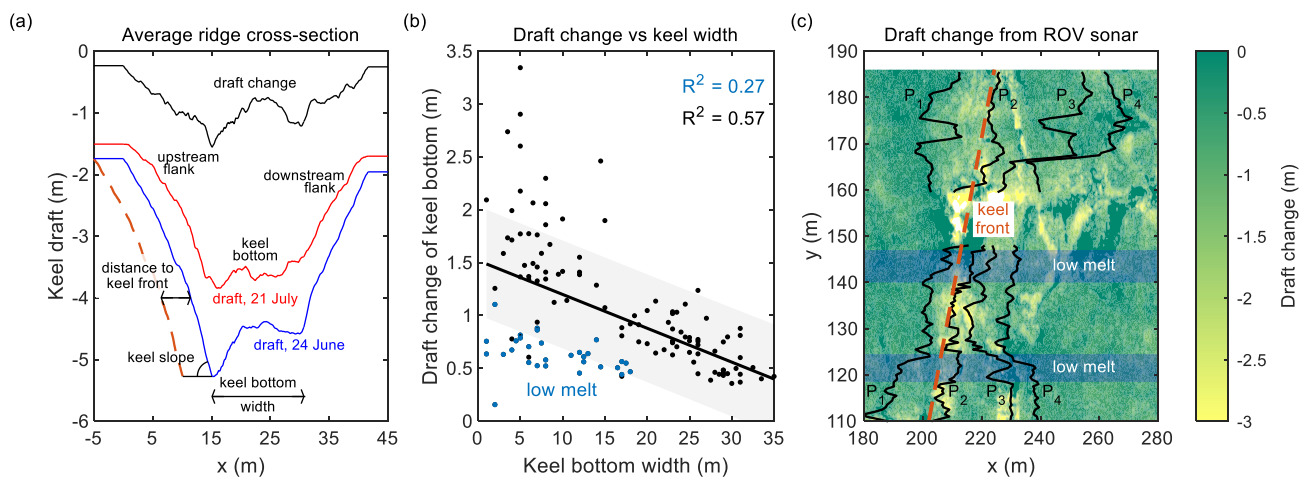
Figure 4: (a) Average ridge cross-section of ice draft in late June and late July 2020; (b) draft change of keel bottom vs keel bottom width for each ridge cross-section; (c) contour plot of ridge draft change from 24 June to 21 July with locations of ridge corners P_{1-4} (black lines), keel front (red dashed line), and cross-sections with low total melt and narrow keel width (blue shaded areas).

3.4 Total, surface and bottom ice melt

225 In the previous sections we analysed draft evolution of several sea-ice types. Under the assumption of hydrostatic equilibrium, the sea-ice draft decrease equals the amount of surface and bottom melt multiplied by snow and sea-ice density, respectively, and divided by water density. Meanwhile, it is important to separate surface and bottom melt to study thermodynamic coupling of sea ice, ocean and atmosphere. From 22 June to 20 July, unponded level ice at the FYI coring site experienced 0.18 m surface melt and 0.14 m bottom melt, with nearly identical draft change (0.34 m) and total melt

230 (0.32 m). Meanwhile, sonar measurements gave a larger FYI draft change (0.41 m), and hence provided a substantially larger estimate of FYI bottom melt (0.25 m). The reason of such difference is discussed in the next two sections.

During the same period, the average snow depth above Jaridge decreased from 0.50 m to 0.12 m. Temperature measurements from IMB indicate surface ridge melt of 0.24 m. Assuming 0.24 m of surface melt and 0.38 m of snowmelt for the whole ridge, using sonar measurements we can estimate the average ridge bottom melt as 0.55 m or 60 % of the mean ridge total

235 melt of 0.93 m. This may explain why only 57 % of the ridge total melt was related to characteristics of the keel topography. The surface melt of level FYI and the ridge was similar, whereas the ridge bottom melt estimates were 2.2–3.9 times larger than for level FYI.

The average ridge macroporosity measured by drilling in June–July was 4±7 % for all 47 drilling sites (Fig. A1). Bottom ridge brine volume (5–7 %) was lower than for FYI due to lower ridge temperatures (Fig. 1a). This shows that the ridge

240 macroporosity and brine volume fraction have a minor effect on the estimate of the total volume of melted ice based on its draft measurements relatively to the difference in melt between various ice types. A study focused on the seasonal evolution of ridge consolidation during MOSAiC showed that the most of consolidation occurred during spring season, while upon melt onset ridges were already fully consolidated (Salganik et al., 2023a).

3.5 Effect of meltwater drainage on ice draft

245 From 7 July to 14 July, we observed abnormal 0.08 m increase of FYI freeboard at the coring site, despite 0.16 m total melt (Fig. 5a). We suggest that this short-term imbalance is related to surface melt pond drainage observed from 9 July to 13 July (Webster et al., 2022), which was accompanied with the formation of an under-ice meltwater layer with 21 % areal coverage and 0.46 m thickness (Salganik et al., 2023b). This suggests that the large decrease in draft (0.30 m) for FYI measured by sonar during 7–14 July was not purely due to ice melt but includes approximately 0.10 m freeboard increase (Fig. 5c).

250 During that period, independent measurements from FYI coring also showed a substantially larger draft decrease (0.24 m in comparison to 0.08 m draft change during 14–21 July). Meanwhile, the total FYI melt from coring during these two weeks was 0.16 m and 0.14 m, respectively. Our observations also indicate that increase of FYI freeboard caused by meltwater drainage was reversible. It is supported by the rapid recovery of surface melt pond fraction and depth to the values prior to drainage during 13–17 July (Webster et al., 2022).

255
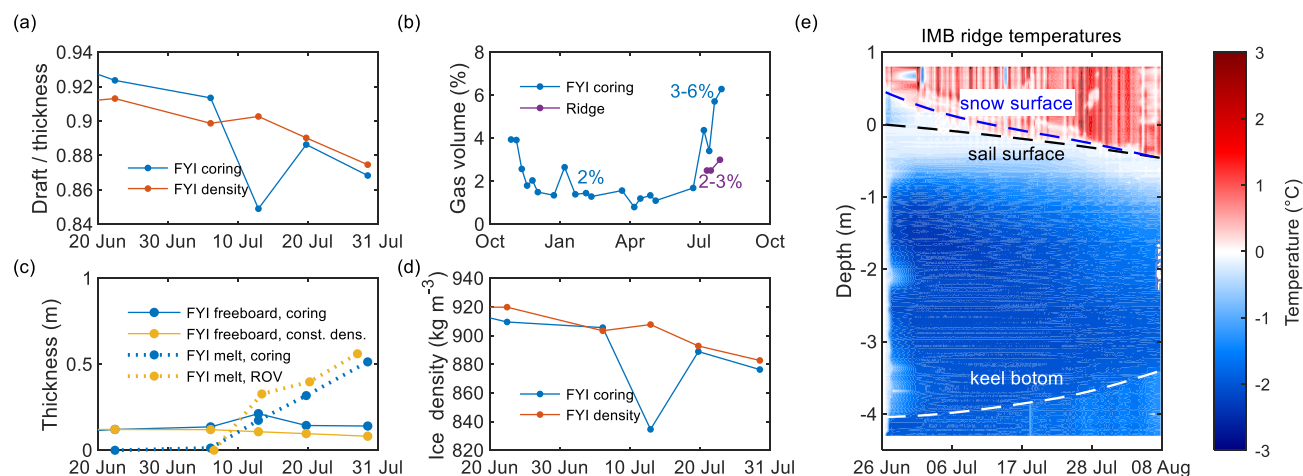
Figure 5: (a) Evolution of first-year ice (FYI) draft and thickness ratio; (b) FYI and ridge gas volume; (c) FYI freeboard and total melt; (d) FYI density estimated from measurements of snow and ice thickness and draft, and from density measurements; (e) contour plot of the ridge temperature measurements from IMB buoy 2020M26.

260 **3.6 Effect of sea-ice density on ice draft**

The relationship between sea-ice draft, freeboard and thickness mainly depends on snow and sea-ice thickness and density. For various remote sensing measurements including satellite altimetry (Landy et al., 2022) and upward looking sonars (Sumata et al., 2023), the sea ice density is assumed constant, while considering sea-ice density seasonal evolution may improve the accuracy of satellite ice thickness retrievals (Fons et al., 2023). For our measurements, the snow at the FYI
265 coring site melted entirely from an initial depth of 0.08 m and had a minor effect on FYI freeboard. Meanwhile, the ratio of FYI draft to thickness gradually decreased from 0.92 on 22 June to 0.87 on 29 July (Fig. 5a). The corresponding estimate of sea-ice bulk density (assuming hydrostatic equilibrium) decreased from 910 kg/m^3 to 876 kg/m^3, which agrees with a sea-ice density decrease from 914 kg/m^3 to 875 kg/m^3 from the direct density measurements performed at the FYI coring site (Fig. 5d), as well as with previous measurements of sea-ice density seasonal evolution (Fons et al., 2023). In these estimates, the
270 gas fraction was calculated from laboratory hydrostatic measurements of sea-ice density, while brine volume was calculated from in situ temperature and salinity measurements. The observed sea-ice density decrease was mainly caused by an increase in gas fraction from 2 % to 6 % (Fig. 5b). We suggest that the decrease of FYI density led to a large difference in FYI melt estimates from coring thickness measurements (0.34 m) and from sonar draft measurements (0.46 m), indicating that the FYI melt from sonar may be overestimated when assuming a constant sea-ice density (Fig. 5c). Measurements from an airborne
275 laser scanner give 0.02 m increase of FYI freeboard during 4–17 July, which agrees with 0.01 m freeboard increase from FYI coring during 6–20 July, supporting our density measurements and upscaling them for the whole FYI area, surveyed by multibeam sonar. A gradual increase of FYI freeboard from 22 June to 29 July by 0.02 m despite a total FYI melt of 0.52 m, observed at FYI coring site and mainly caused by the decrease of FYI density, may affect aerial and satellite altimetry retrievals in Arctic summer.

280   Unlike for the level ice, the ratio of draft to thickness for Jaridge was 0.89±0.06 and did not decrease (Fig. A1), while the
       ridge bulk density estimated from coring measurements on 10 July was 892 kg/m^3. The ridge gas volume fraction was 2.5–
       3.0 % (Fig. 5b). The absence of ridge lift during melt season is supported by sonar measurements with smaller draft change
       of FYI and SYI (0.24–0.25 m) right next to the ridge in comparison to the average FYI and SYI draft change of 0.41–0.50 m
       away from the ridge. These measurements suggest modification of draft to thickness ratio for analysis of sonar surveys

285   depending on sea-ice density and ice type. Therefore, we suggest 3.8 times higher bottom and 3.0 times higher total melt
       rates for the sea-ice ridge than for FYI. For a typical areal fraction of sea-ice ridges (40–50 %), we estimate that they
       produce 1.7–2.5 times more meltwater that level ice.

       Measurements of sea-ice bottom melt allow to estimate the OHF for different ice types following Shestov et al. (2018). From
       24 June to 21 July, calculations based on temperature measurements from the FYI IMB result in an average OHF of 17 W m^{-2}

290   ^{2}, increasing from 11 W m^{-2} to 36 W m^{-2} (Salganik et al., 2023b). A combination of sonar and IMB measurements at the
       ridge result in an average OHF of 65 W m^{-2} with averages of 20 W m^{-2} during 24 June – 7 July and 107 W m^{-2} during 8 July
       – 21 July, respectively, suggesting larger ridge melt enhancement for lower sea-ice concentrations due to increased solar heat
       input.

       ### 3.7 Comparison with previous observations of enhanced ridge melt

295   The areas representative for the Arctic sea ice cover are characterized by high ice concentration and comparable surface and
       bottom level ice melt, while the largest amount of bottom level ice melt occurs in regions with low ice concentration
       (Perovich et al., 2011). The average accumulated surface/bottom melt of level ice was 0.56/0.50 m for yearlong SHEBA
       measurements and 0.24/0.31 m for MOSAiC, with measurements until 29 July, covering approximately half of the SHEBA
       melt season. The average OHF was 18 W m^{-2} from 3 June to 4 October for SHEBA and 18 W m^{-2} from 3 June to 29 July for

300   MOSAiC FYI coring site, similar to the average summer estimates for Beaufort Gyre and Transpolar Drift (Krishfield,
       2005). This suggests that level ice melt during MOSAiC was comparable to SHEBA with surface and bottom melt ratio
       typical for areas with high ice concentration. Despite deeper ridge keel with a 6 m average draft on SHEBA, the enhanced
       ridge bottom melt relative to level ice was only 60 % in comparison to 280 % for MOSAiC with average keel bottom draft of
       5.3 m. This difference may be related to the larger (second-year and multiyear) age of SHEBA ridges or to the substantially

305   smaller areal coverage of SHEBA ridge measurements with only 14 stakes at the second-year ridge in comparison to over
       10^4 ridge draft measurements for MOSAiC, with the latter capturing the whole range of different melt rates.

       The oceanographic conditions during N-ICE2015 were substantially different from both SHEBA and MOSAiC due to the
       proximity to Atlantic Water, with the average OHF under level ice of 63 W m^{-2} during 10–19 June 2015 (Peterson et al.,
       2017), six times higher than for MOSAiC during the same period. The enhanced OHF for ice ridges during N-ICE2015,

310   observed by Shestov et al. (2018), is based on one single-point measurement of bottom ridge melt from a temperature buoy
       and OHF estimate from turbulence instrument clusters for level ice. The keel macroporosity of the ridge studied by Shestov
       et al. (2018) was 8 % (higher than 4 % for MOSAiC, possibly due to lower N-ICE2015 keel width of 16 m), the maximum

keel depth was 7.3 m, and the estimated increase of the ridge bottom melt in comparison to level ice was 4.8 compared to 3.8 for MOSAiC. The enhanced first-year ridge melt estimated from draft measurements from upward looking sonar in Beaufort

315 Sea from Amundrud et al. (2006) may have substantial uncertainties as they are based on an assumption of similar ice draft distribution along the direction of ice drift (and not necessarily repeated measurements of the same ridges), while ridge macroporosity, block thickness, sea-ice density, and fraction of surface and bottom ice melt were unknown. Amundrud et al. (2006) estimated the total level ice melt rate in July as 0.02–0.03 m d^{-1}, higher than 0.018 m d^{-1} for MOSAiC FYI coring site (1–29 July), while the total melt rate for ridges with 4–8 m draft was 0.10 m d^{-1} in Beaufort Sea and 0.04 m d^{-1} during

320 MOSAiC (1–21 July). The corresponding ridge melt enhancement of 4.0 was higher than the ratio of ridge and level ice total melt of 3.0 for MOSAiC. Another ridge (Alli's Ridge) with similar block thickness, keel draft, width, and macroporosity, but oriented along the drift direction (perpendicular to Jaridge), was studied during MOSAiC. Despite different orientation, Alli's ridge experienced similar draft decrease of 0.9 m as Jaridge, however, those observations are limited to four point-measurements across a single ridge cross-section.

325 The results of our sonar investigations provided evidence of high spatial variability of sea ice melt, especially for ridges. For the ridge with total cross-sectional melt of 0.9±0.4 m, we identified cross-sections with an average total melt ranging from 0.2 m to 2.6 m. This means that measurements from a single location or an even single ridge cross-section may be not representative, as variability of draft change is comparable to the difference between average melt of different sea-ice types. This suggests that 20–30 % difference between our observations of first-year ridge enhanced melt and observations from

330 Amundrud et al. (2006) and Shestov et al. (2018) may be related to the high spatial variability of ridge melt or different oceanographic conditions, while much larger 120 % difference from Perovich et al. (2003) may be attributed to different ridge age, as second- and multiyear ice ridges surveyed in their study were typically smooth and fully consolidated (Kovacs et al., 1973).

3.3 Study application and limitations

335 Our study provides melt estimates for different ice types over a substantial range of sea ice draft. It also describes effects of ridge morphological parameters including ridge draft, slope and width on melt rates. This allows to extrapolate our estimates on a range of ridge cross-sections with various shapes and draft. Nevertheless, we acknowledge limitations related to some other ridge characteristics which may affect melt, such as macroporosity, the block thickness, and the ridge age. Most of characteristics of the investigated ridge are close to the average characteristics of first-year ice ridges with 8 m maximum

340 keel depth, 36 m keel width and 0.2–0.4 m block thickness (Strüb-Klein and Høyland, 2011), except for its low macroporosity (amount of ridges sampled during the melt season is limited, but melting ridges often have low macroporosity (Marchenko, 2022; Shestov et al., 2018)). Previous studies on the ridge melt showed a wide range of ridge and level ice melt fraction from only 1.6 (Perovich et al., 2003) to 4–5 (Amundrud et al., 2006; Shestov et al., 2018), yet due to limited coverage of these observations, it is challenging to indicate, which parameters were the main reason for such differences in

345 ridge melt.

4 Conclusions

We collected an unprecedented dataset using a multibeam sonar mounted on an ROV that captured the four-dimensional change of sea-ice draft over a period of one month during advanced summer melt in the Arctic Ocean. This revealed that a first-year ridge with an average draft of 3.9 m melted faster than adjacent level ice types. The total ridge melt was on average

350   0.95 m, compared to 0.55 m for level second-year ice and 0.46 m for level first-year ice. These observations can largely be explained by the difference in initial average ice draft, of 1.4 m for first-year ice, 2.6 m for second-year ice, and 3.9 m for the ridge. Ridge bottom melt was 4 times higher than bottom melt of first-year level ice, while surface melt was almost identical. Key factors that affect the melt rates of ridge keels, included the keel draft, slope, width, and distance from the keel front. These factors can explain 57 % of the total melt variability for this particular ridge, with 36 % of the melt variability

355   explained by keel draft, 32 % by keel slope, 27 % by keel width, and 11 % by a distance from the keel front. We observed a relationship between the melt of ridge flanks with their draft, and amplification of keel melt within 10 m of its bottom corners, while melt rates of the (more level) middle part of ridge keel were comparable to level ice melt. However, ice draft changes (as measured by sonars) are not due to ice melt alone, because the hydrostatic balance of the ice needs to be considered, since, e.g., melt pond drainage and sea-ice density evolution change ice draft. This needs to be considered when

360   such measurements are used over longer periods of time. Considering sea-ice density seasonal evolution allowed us to refine the ratio of total ridge to first-year level ice melt to 3.0. Such ice draft changes also affect the ice freeboard and can potentially affect satellite altimetry retrievals in Arctic summer.

Since a large fraction of the Arctic ice pack is deformed (ridged) ice, it is imperative that we better understand their role in the Arctic sea-ice system. While ridge keels contribute a significant amount of ice melt in summer (Perovich et al., 2021),

365   they also provide a sink for meltwater through refreezing in keel voids (Lange et al., 2023). Ridge keels also shape the lateral distribution of under-ice meltwater layers (which in turn affect level ice melt rates) (Salganik et al., 2023b) and affects turbulent exchanges (Skyllingstad et al., 2003), with implications for ice-ocean exchange. This work highlights areas that warrant future observation-model development for improved representation of ridge related sea-ice processes in models.

Appendix A: Additional information
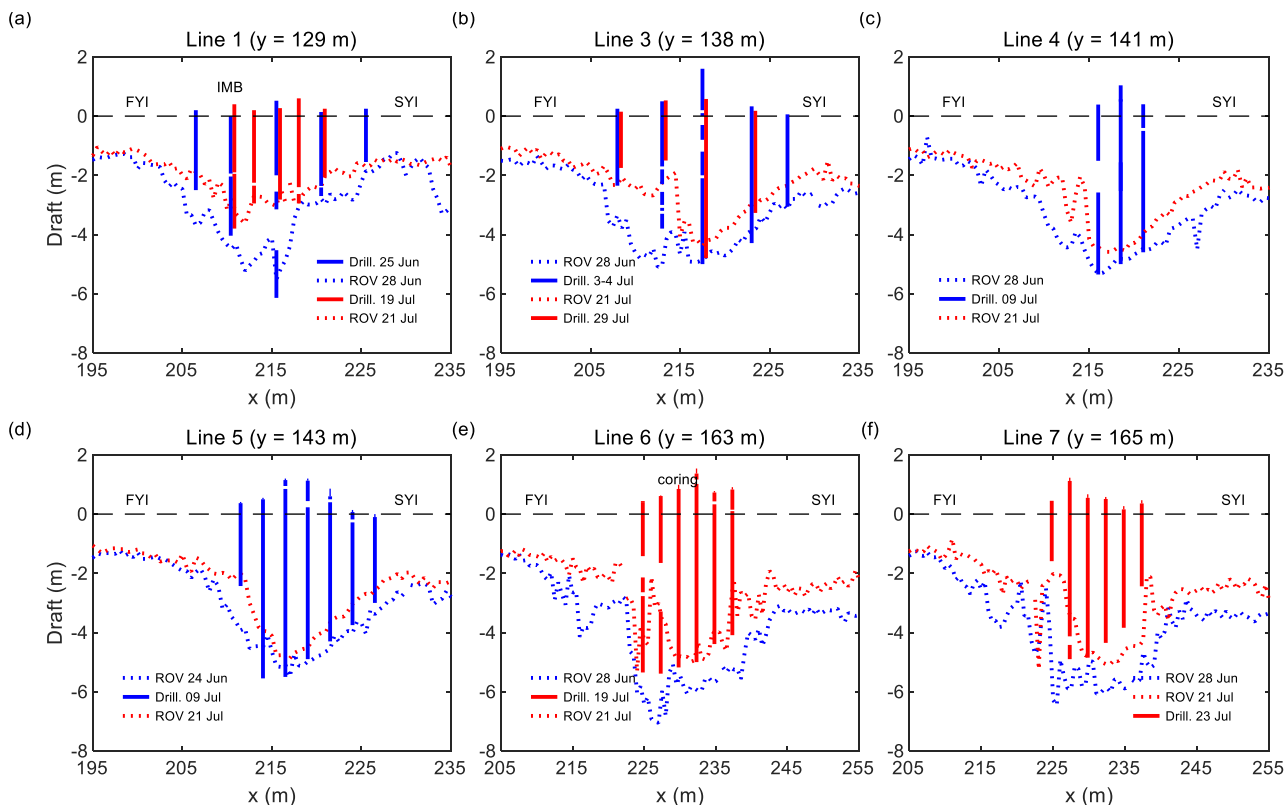
370

Figure A1: Ridge draft measurements from ROV multibeam sonar and ice drilling lines.
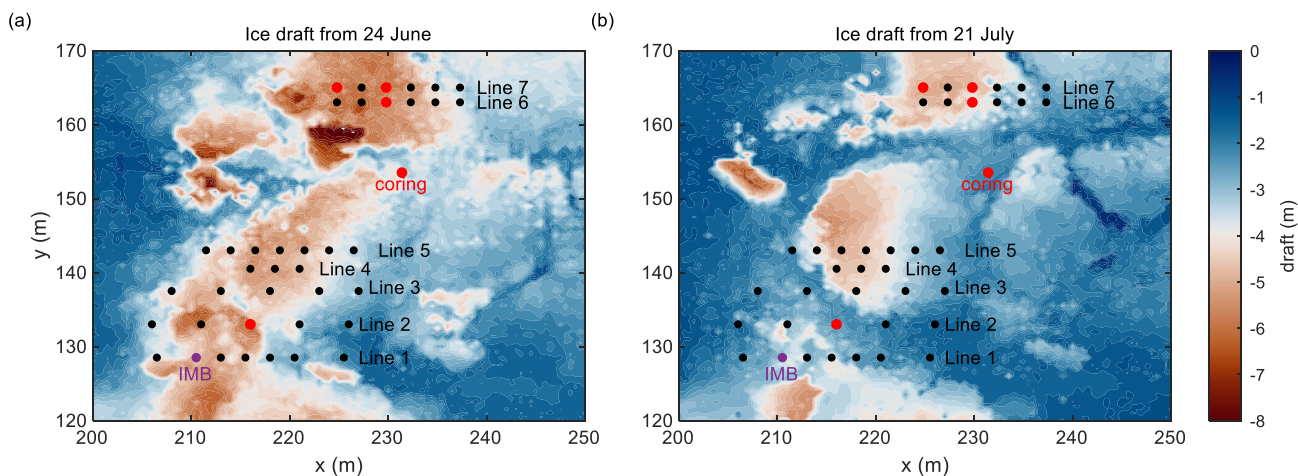
Figure A2: Contour plot with ice draft for 24 June (a) and 21 July (b). Black points show ridge drilling locations, purple point shows the location of ice mass balance buoy (IMB), and red points show the location of ridge coring. Contour plot colours follow
375 **recommendations of scientifically derived colour maps (Crameri et al., 2020).**

Data availability

All scientific data used in this study is publicly available:

Granskog, M. A.; Lange, B. A., Salganik, E., De La Torre, P. R., Riemann-Campe, K.: Temperature and heating induced temperature difference measurements from the modular buoy 2020M26, deployed during MOSAiC 2019/20. *PANGAEA*,

380   https://doi.org/10.1594/PANGAEA.938354, 2021.

Jutila, A., Hendricks, S., Birnbaum, G., von Albedyll, L., Ricker, R., Helm, V., Hutter, N., Haas, C.: Geolocated sea-ice or snow surface elevation point cloud segments from helicopter-borne laser scanner during the MOSAiC expedition, version 1. *PANGAEA*, https://doi.pangaea.de/10.1594/PANGAEA.950509, 2022.

Katlein, C., Anhaus P., Arndt S., Krampe, D., Lange, B. A., Matero, I., Regnery, J., Rohde, J., Schiller, M., Nicolaus, M.:

385   Sea-ice draft during the MOSAiC expedition 2019/20. *PANGAEA*, https://doi.org/10.1594/PANGAEA.945846, 2022.

Lange, B. A., Salganik, E., Macfarlane, A. R., Schneebeli, M., Høyland, K. V., Gardner, J., Müller, O., Granskog, M. A.: Ridge ice oxygen and hydrogen isotope data MOSAiC Leg 4 (PS122/4). *PANGAEA*, https://doi.org/10.1594/PANGAEA.943746, 2022.

Neckel, N., Fuchs, N., Birnbaum, G., Hutter, N., Jutila, A., Buth, L., von Albedyll, L., Ricker, R., Haas, C.: Helicopter-borne

390   RGB orthomosaics and photogrammetric Digital Elevation Models from the MOSAiC Expedition. *PANGAEA*, https://doi.pangaea.de/10.1594/PANGAEA.949433, 2022.

Oggier, M., Salganik, E., Whitmore, L., Fong, A. A., Hoppe, C. J. M., Rember, R., Høyland, K. V., Divine, D. V., Fons, S. W., Abrahamsson, K., Aguilar-Islas, A. M., Angelopoulos, M., Balmonte, J. P., Bozzato, D., Bowman, J. S., Chamberlain, E., Creamean, J., D'Angelo, A., Gardner, J., Haapala, J., Immerz, A., Kolabutin, N., Lange, B. A., Lei, R., Marsay, C. M.,

395   Maus, S., Olsen, L. M., Müller, O., Ren, J., Rinke, A., Sheikin, I., Shimanchuk, E., Spahic, S., Torres-Valdés, S., Torstensson, A., Ulfsbo, A., Wang, L., Granskog, M. A.: First-year sea-ice salinity, temperature, density, oxygen and hydrogen isotope composition from the main coring site (MCS-FYI) during MOSAiC legs 1 to 4 in 2019/2020. PANGAEA, https://doi.pangaea.de/10.1594/PANGAEA.956732, 2023.

Salganik, E., Lange, B. A., Sheikin, I., Høyland, K. V., Granskog, M. A. (2023). Drill-hole ridge ice and snow thickness and

400   draft measurements of "Jaridge" during MOSAiC 2019/20. *PANGAEA*, https://doi.org/10.1594/PANGAEA.953880

Salganik, E., Lange, B. A., Høyland, K. V., Gardner, J., Müller, O., Tavri, A., Mahmud, M. Granskog, M.A.: Ridge ice density data MOSAiC Leg 4 (PS122/4). PANGAEA, https://doi.org/10.1594/PANGAEA.953865, 2023.

Schmithüsen, H. 2021. Continuous meteorological surface measurement during POLARSTERN cruise PS122/4. Alfred Wegener Institute, Helmholtz Centre for Polar and Marine Research, Bremerhaven, PANGAEA,

405   https://doi.org/10.1594/PANGAEA.935224.

Schulz, K., Mohrholz, V., Fer, I., Janout, M. A., Hoppmann, M., Schaffer, J., Koenig, Z., Rabe, B., Heuzé, C., Regnery, J., Allerholt, J., Fang, Y.-C., He, H., Kanzow, T., Karam, S., Kuznetsov, I. Kong, B., Liu, H., Muilwijk, M., Schuffenhauer, I.,

Sukhikh, N., Sundfjord, A., Tippenhauer, S.: Turbulent microstructure profile (MSS) measurements from the MOSAiC drift, Arctic Ocean. *PANGAEA*, https://doi.org/10.1594/PANGAEA.939816, 2022.

Author contribution

ES, BAL, CK, IM, KVH and MAG contributed to the design of the study. ES, BAL, CK, IM and MM collected and processed the field data. ES undertook the statistical analyses and interpreted the results. ES and MAG prepared the manuscript with contributions from all co-authors.

Competing interests

The authors declare that they have no conflict of interest.

Acknowledgments

This work was carried out and data used in this manuscript was produced as part of the international Multidisciplinary drifting Observatory for the Study of the Arctic Climate (MOSAiC) with the tag MOSAiC20192020. We thank all persons involved in the expedition of the Research Vessel *Polarstern* (Alfred-Wegener-Institut Helmholtz-Zentrum für Polar- und Meeresforschung, 2017) during MOSAiC in 2019–2020 (Project_ID: AWI_PS122_00) as listed in Nixdorf et al. (2021). We would especially like to acknowledge Marcel Nicolaus and Donald Perovich for their effort to coordinate the sea ice physics work during MOSAiC. We are grateful to Marcel Nicolaus for his effort to coordinate ROV work during MOSAiC. We thank Julia Regnery for the assistance with ROV multibeam sonar measurements and ROV co-piloting. We are grateful for the assistance of Niklas Neckel in processing MOSAiC Helicopter-borne RGB orthomosaics.

ES, BAL, KVH, and MAG were supported by the Research Council of Norway through project HAVOC (grant no 280292). ES was also supported by Research Council of Norway project INTERAAC (grant no 328957), BAL and MAG by Research Council of Norway project CAATEX (grant no 280531) and MAG and MM by the Norwegian Polar Institute. MAG and MM received funding from the European Union's Horizon 2020 research and innovation programme (grant agreement No 101003826) via project CRiceS (Climate Relevant interactions and feedbacks: the key role of sea ice and Snow in the polar and global climate system). ROV operations, IM and CK were jointly supported by UKRI Natural Environment Research Council (NERC) and the German Federal Ministry of Education and Research (BMBF) through the Diatom ARCTIC project (BMBF Grant 03F0810A). ROV operations were further supported by the Helmholtz Infrastructure Initiative Frontiers in Arctic marine Monitoring (FRAM). PA was supported through the Alfred-Wegener-Institutes internal project AWI_ROV and BMBF through the Diatom ARCTIC project (BMBF Grant 03F0810A) and the IceScan project (BMBF Grant 03F0916A).

References

Amundrud, T. L., Melling, H., and Ingram, G.: Geometrical constraints on the evolution of ridged sea ice, J. Geophys. Res. Ocean., 109, 1–12, https://doi.org/10.1029/2003JC002251, 2004.

Amundrud, T. L., Melling, H., Ingram, R. G., and Allen, S. E.: The effect of structural porosity on the ablation of sea ice ridges, J. Geophys. Res., 111, C06004, https://doi.org/10.1029/2005JC002895, 2006.

Bowen, R. G. and Topham, D. R.: A study of the morphology of a discontinuous section of a first year arctic pressure ridge, Cold Reg. Sci. Technol., 24, 83–100, https://doi.org/10.1016/0165-232X(95)00002-S, 1996.

Crameri, F., Shephard, G. E., and Heron, P. J.: The misuse of colour in science communication, Nat. Commun., 11, 5444, https://doi.org/10.1038/s41467-020-19160-7, 2020.

Ekeberg, O., Høyland, K., and Hansen, E.: Ice ridge keel geometry and shape derived from one year of upward looking sonar data in the Fram Strait, Cold Reg. Sci. Technol., 109, 78–86, https://doi.org/10.1016/j.coldregions.2014.10.003, 2015.

Fer, I., Baumann, T. M., Koenig, Z., Muilwijk, M., and Tippenhauer, S.: Upper-Ocean Turbulence Structure and Ocean-Ice Drag Coefficient Estimates Using an Ascending Microstructure Profiler During the MOSAiC Drift, J. Geophys. Res. Ocean., 127, 1–23, https://doi.org/10.1029/2022JC018751, 2022.

Fernández-Méndez, M., Olsen, L. M., Kauko, H. M., Meyer, A., Rösel, A., Merkouriadi, I., Mundy, C. J., Ehn, J. K., Johansson, A. M., Wagner, P. M., Ervik, Å., Sorrell, B. K., Duarte, P., Wold, A., Hop, H., and Assmy, P.: Algal hot spots in a changing Arctic Ocean: sea-ice ridges and the snow-ice interface, Front. Mar. Sci., 5, https://doi.org/10.3389/fmars.2018.00075, 2018.

Fons, S., Kurtz, N., and Bagnardi, M.: A decade-plus of Antarctic sea ice thickness and volume estimates from CryoSat-2 using a physical model and waveform fitting, Cryosph., 17, 2487–2508, https://doi.org/10.5194/tc-17-2487-2023, 2023.

Gradinger, R., Bluhm, B., and Iken, K.: Arctic sea-ice ridges—Safe heavens for sea-ice fauna during periods of extreme ice melt?, Deep Sea Res. Part II Top. Stud. Oceanogr., 57, 86–95, https://doi.org/10.1016/j.dsr2.2009.08.008, 2010.

Granskog, M. A., Fer, I., Rinke, A., and Steen, H.: Atmosphere-ice-ocean-ecosystem processes in a thinner Arctic sea ice regime: the Norwegian Young Sea ICE (N-ICE2015) Expedition, J. Geophys. Res. Ocean., 123, 1586–1594, https://doi.org/10.1002/2017JC013328, 2018.

Hansen, E., Ekeberg, O. -C., Gerland, S., Pavlova, O., Spreen, G., and Tschudi, M.: Variability in categories of Arctic sea ice in Fram Strait, J. Geophys. Res. Ocean., 119, 7175–7189, https://doi.org/10.1002/2014JC010048, 2014.

Hopkins, M. A.: Four stages of pressure ridging, J. Geophys. Res. Ocean., 103, 21883–21891, https://doi.org/10.1029/98JC01257, 1998.

Katlein, C., Schiller, M., Belter, H. J., Coppolaro, V., Wenslandt, D., and Nicolaus, M.: A New Remotely Operated Sensor Platform for Interdisciplinary Observations under Sea Ice, Front. Mar. Sci., 4, 1–12, https://doi.org/10.3389/fmars.2017.00281, 2017.

Katlein, C., Langelier, J., Ouellet, A., Lévesque-Desrosiers, F., Hisette, Q., Lange, B. A., Lambert-Girard, S., Babin, M., and

Thibault, S.: The Three-Dimensional Light Field Within Sea Ice Ridges, Geophys. Res. Lett., 48, https://doi.org/10.1029/2021GL093207, 2021.

470 Kovacs, A., Weeks, W. F., Ackley, S., and Hibler, W. D.: Structure of a Multi-Year Pressure Ridge, ARCTIC, 26, https://doi.org/10.14430/arctic2893, 1973.

Krishfield, R. A.: Spatial and temporal variability of oceanic heat flux to the Arctic ice pack, J. Geophys. Res., 110, C07021, https://doi.org/10.1029/2004JC002293, 2005.

Krumpen, T., Gerdes, R., Haas, C., Hendricks, S., Herber, A., Selyuzhenok, V., Smedsrud, L., and Spreen, G.: Recent 475 summer sea ice thickness surveys in Fram Strait and associated ice volume fluxes, Cryosphere, 10, 523–534, https://doi.org/10.5194/tc-10-523-2016, 2016.

Krumpen, T., von Albedyll, L., Goessling, H. F., Hendricks, S., Juhls, B., Spreen, G., Willmes, S., Belter, H. J., Dethloff, K., Haas, C., Kaleschke, L., Katlein, C., Tian-Kunze, X., Ricker, R., Rostosky, P., Rückert, J., Singha, S., and Sokolova, J.: MOSAiC drift expedition from October 2019 to July 2020: sea ice conditions from space and comparison with previous 480 years, Cryosph., 15, 3897–3920, https://doi.org/10.5194/tc-15-3897-2021, 2021.

Landy, J. C., Dawson, G. J., Tsamados, M., Bushuk, M., Stroeve, J. C., Howell, S. E. L., Krumpen, T., Babb, D. G., Komarov, A. S., Heorton, H. D. B. S., Belter, H. J., and Aksenov, Y.: A year-round satellite sea-ice thickness record from CryoSat-2, Nature, 609, 517–522, https://doi.org/10.1038/s41586-022-05058-5, 2022.

Lange, B. A., Salganik, E., Macfarlane, A., Schneebeli, M., Høyland, K., Gardner, J., Müller, O., Divine, D. V., Kohlbach, 485 D., Katlein, C., and Granskog, M. A.: Snowmelt contribution to Arctic first-year ice ridge mass balance and rapid consolidation during summer melt, Elem Sci Anth, 11, https://doi.org/10.1525/elementa.2022.00037, 2023.

Lyon, W.: Ocean and sea-ice research in the Arctic Ocean via submarine, Trans. N. Y. Acad. Sci., 23, 662–674, https://doi.org/10.1111/j.2164-0947.1961.tb01400.x, 1961.

Marchenko, A.: Thermo-Hydrodynamics of Sea Ice Rubble, Springer International Publishing, 203–223 pp., 490 https://doi.org/10.1007/978-3-030-80439-8_10, 2022.

Mårtensson, S., Meier, H. E. M., Pemberton, P., and Haapala, J.: Ridged sea ice characteristics in the Arctic from a coupled multicategory sea ice model, J. Geophys. Res. Ocean., 117, https://doi.org/10.1029/2010JC006936, 2012.

Melling, H. and Riedel, D. A.: Development of seasonal pack ice in the Beaufort Sea during the winter of 1991-1992: A view from below, J. Geophys. Res. Ocean., 101, 11975–11991, https://doi.org/10.1029/96JC00284, 1996.

495 Nicolaus, M., Perovich, D. K., Spreen, G., Granskog, M. A., von Albedyll, L., Angelopoulos, M., Anhaus, P., Arndt, S., Belter, H. J., Bessonov, V., Birnbaum, G., Brauchle, J., Calmer, R., Cardellach, E., Cheng, B., Clemens-Sewall, D., Dadic, R., Damm, E., de Boer, G., Demir, O., Dethloff, K., Divine, D. V., Fong, A. A., Fons, S., Frey, M. M., Fuchs, N., Gabarró, C., Gerland, S., Goessling, H. F., Gradinger, R., Haapala, J., Haas, C., Hamilton, J., Hannula, H.-R., Hendricks, S., Herber, A., Heuzé, C., Hoppmann, M., Høyland, K. V., Huntemann, M., Hutchings, J. K., Hwang, B., Itkin, P., Jacobi, H.-W., Jaggi, 500 M., Jutila, A., Kaleschke, L., Katlein, C., Kolabutin, N., Krampe, D., Kristensen, S. S., Krumpen, T., Kurtz, N., Lampert, A., Lange, B. A., Lei, R., Light, B., Linhardt, F., Liston, G. E., Loose, B., Macfarlane, A. R., Mahmud, M., Matero, I. O., Maus,

S., Morgenstern, A., Naderpour, R., Nandan, V., Niubom, A., Oggier, M., Oppelt, N., Pätzold, F., Perron, C., Petrovsky, T., Pirazzini, R., Polashenski, C., Rabe, B., Raphael, I. A., Regnery, J., Rex, M., Ricker, R., Riemann-Campe, K., Rinke, A., Rohde, J., Salganik, E., Scharien, R. K., Schiller, M., Schneebeli, M., Semmling, M., Shimanchuk, E., Shupe, M. D., Smith,

505   M. M., Smolyanitsky, V., Sokolov, V., Stanton, T., Stroeve, J., Thielke, L., Timofeeva, A., Tonboe, R. T., Tavri, A., et al.: Overview of the MOSAiC expedition, Elem. Sci. Anthr., 10, https://doi.org/10.1525/elementa.2021.000046, 2022.

Perovich, D., Smith, M., Light, B., and Webster, M.: Meltwater sources and sinks for multiyear Arctic sea ice in summer, Cryosphere, 15, 4517–4525, https://doi.org/10.5194/tc-15-4517-2021, 2021.

Perovich, D. K., Grenfell, T. C., Richter-Menge, J. A., Light, B., Tucker, W. B., and Eicken, H.: Thin and thinner: Sea ice

510   mass balance measurements during SHEBA, J. Geophys. Res. Ocean., 108, 1–21, https://doi.org/10.1029/2001jc001079, 2003.

Perovich, D. K., Richter-Menge, J. A., Jones, K. F., Light, B., Elder, B. C., Polashenski, C., Laroche, D., Markus, T., and Lindsay, R.: Arctic sea-ice melt in 2008 and the role of solar heating, Ann. Glaciol., 52, 355–359, https://doi.org/10.3189/172756411795931714, 2011.

515   Peterson, A. K., Fer, I., McPhee, M. G., and Randelhoff, A.: Turbulent heat and momentum fluxes in the upper ocean under Arctic sea ice, J. Geophys. Res. Ocean., 122, 1439–1456, https://doi.org/10.1002/2016JC012283, 2017.

Rigby, F. A. and Hanson, A.: Evolution of a large Arctic pressure ridge, AIDJEX Bull., 34, 43–71, 1976.

Rothrock, D. A.: Arctic Ocean sea ice volume: What explains its recent depletion?, J. Geophys. Res., 110, C01002, https://doi.org/10.1029/2004JC002282, 2005.

520   Salganik, E., Lange, B. A., Itkin, P., Divine, D., Katlein, C., Nicolaus, M., Hoppmann, M., Neckel, N., Ricker, R., Høyland, K. V., and Granskog, M. A.: Different mechanisms of Arctic first-year sea-ice ridge consolidation observed during the MOSAiC expedition, Elem Sci Anth, 11, https://doi.org/10.1525/elementa.2023.00008, 2023a.

Salganik, E., Katlein, C., Lange, B. A., Matero, I., Lei, R., Fong, A. A., Fons, S. W., Divine, D., Oggier, M., Castellani, G., Bozzato, D., Chamberlain, E. J., Hoppe, C. J. M., Müller, O., Gardner, J., Rinke, A., Pereira, P. S., Ulfsbo, A., Marsay, C.,

525   Webster, M. A., Maus, S., Høyland, K. V., and Granskog, M. A.: Temporal evolution of under-ice meltwater layers and false bottoms and their impact on summer Arctic sea ice mass balance, Elem. Sci. Anthr., 11, https://doi.org/10.1525/elementa.2022.00035, 2023b.

Schulz, K., Koenig, Z., and Muilwijk, M.: The Eurasian Arctic Ocean along the MOSAiC drift (2019-2020): Properties and processes, from the dynamic surface to the deep, in prep., 2023.

530   Shestov, A., Høyland, K., and Ervik, Å.: Decay phase thermodynamics of ice ridges in the Arctic Ocean, Cold Reg. Sci. Technol., 152, 23–34, https://doi.org/10.1016/j.coldregions.2018.04.005, 2018.

Skyllingstad, E. D., Paulson, C. A., and Pegau, W. S.: Effects of keels on ice bottom turbulence exchange, J. Geophys. Res., 108, 3372, https://doi.org/10.1029/2002JC001488, 2003.

Spreen, G., Kaleschke, L., and Heygster, G.: Sea ice remote sensing using AMSR-E 89-GHz channels, J. Geophys. Res.,

535   113, C02S03, https://doi.org/10.1029/2005JC003384, 2008.

Strüb-Klein, L. and Høyland, K.: One season of a 1st year sea ice ridge investigation–Winter 2009, Proc. 21st Int. Conf. Port Ocean Eng. under Arct. Cond., 2011.

Sumata, H., de Steur, L., Divine, D. V., Granskog, M. A., and Gerland, S.: Regime shift in Arctic Ocean sea ice thickness, Nature, 615, 443–449, https://doi.org/10.1038/s41586-022-05686-x, 2023.

540 Timco, G. W. and Burden, R. P.: An analysis of the shapes of sea ice ridges, Cold Reg. Sci. Technol., 25, 65–77, https://doi.org/10.1016/S0165-232X(96)00017-1, 1997.

Tucker, W. B., Sodhi, D. S., and Govoni, J. W.: Structure of first-year pressure ridge sails in the Prudhoe region, in: The Alaskan Beaufort Sea, Elsevier, 115–135, https://doi.org/10.1016/B978-0-12-079030-2.50012-5, 1984.

Wadhams, P. and Doble, M. J.: Digital terrain mapping of the underside of sea ice from a small AUV, Geophys. Res. Lett.,
545 35, L01501, https://doi.org/10.1029/2007GL031921, 2008.

Wadhams, P. and Toberg, N.: Changing characteristics of arctic pressure ridges, Polar Sci., 6, 71–77, https://doi.org/10.1016/j.polar.2012.03.002, 2012.

Wadhams, P., Wilkinson, J. P., and McPhail, S. D.: A new view of the underside of Arctic sea ice, Geophys. Res. Lett., 33, L04501, https://doi.org/10.1029/2005GL025131, 2006.

550 Webster, M. A., Holland, M., Wright, N. C., Hendricks, S., Hutter, N., Itkin, P., Light, B., Linhardt, F., Perovich, D. K., Raphael, I. A., Smith, M. M., von Albedyll, L., and Zhang, J.: Spatiotemporal evolution of melt ponds on Arctic sea ice, Elem. Sci. Anthr., 10, https://doi.org/10.1525/elementa.2021.000072, 2022.

WMO: World Meteorological Organization (WMO) Sea Ice Nomenclature: WMO-No. 259 922. Supplement to Vol. I, II and II, 5th session of JCOMM Expert Team on Sea ice. Tech. rep., https://doi.org/10.25607/OBP-1530, 2014.

555